Biophysical Journal
Article

Biophysical Society

Direct Tracking of Particles and Quantification of Margination in Blood Flow

Erik J. Carboni,[1] Brice H. Bognet,[2] Grant M. Bouchillon,[3] Andrea L. Kadilak,[1] Leslie M. Shor,[1,4] Michael D. Ward,[1] and Anson W. K. Ma[1,2,*]

[1]Department of Chemical and Biomolecular Engineering, [2]Polymer Program, Institute of Materials Science, [3]Department of Civil and Environmental Engineering, and [4]Center for Environmental Sciences and Engineering, University of Connecticut, Storrs, Connecticut

ABSTRACT Margination refers to the migration of particles toward blood vessel walls during blood flow. Understanding the mechanisms that lead to margination will aid in tailoring the attributes of drug-carrying particles for effective drug delivery. Most previous studies evaluated the margination propensity of these particles via an adhesion mechanism, i.e., by measuring the number of particles that adhered to the channel wall. Although particle adhesion and margination are related, adhesion also depends on other factors. In this study, we quantified the margination propensity of particles of varying diameters (0.53, 0.84, and 2.11 μm) and apparent wall shear rates (30, 61, and 121 s^{-1}) by directly tracking fluorescent particles flowing through a microfluidic channel. The margination parameter, *M*, is defined as the total number of particles found within the cell-free layers normalized by the total number of particles that passed through the channel. In this study, an *M*-value of 0.2 indicated no margination, which was observed for all particle sizes in water. In the case of blood, larger particles were found to have higher *M*-values and thus marginated more effectively than smaller particles. The corresponding *M*-values at the device outlet were 0.203, 0.223, and 0.285 for 0.53-, 0.84-, and 2.11-μm particles, respectively. At the inlet, the *M*-values for all particle sizes in blood were <0.2, suggesting that non-fully-developed flow and constriction may lead to demargination. For particle velocities transverse to the flow direction (v_y), all particle sizes showed a larger standard deviation of v_y as well as a higher effective diffusivity when the particles were suspended in blood relative to water. These higher values are attributed to collisions between the blood cells and particles, further supporting recent simulation results. In terms of flow rates, for a given particle size, the higher the flow rate, the higher the *M*-value.

INTRODUCTION

Margination refers to the movement of a particle toward the wall of a channel. It was first observed in 1824 for white blood cells (WBCs) in the blood vessels of tadpole tails (1). However, margination is not limited to WBCs and has been observed for other particles as well (2). This has sparked a lot of interest because of its potential applications in relation to cancer therapy (3–7). Tumor sites are generally characterized by 1) leaky vasculature, which allows drug-carrying particles to diffuse into them, and 2) a lack of lymphatics, which allows these particles to remain inside the tumor. This so-called enhanced permeability and retention effect (8) further opens up the possibility of delivering chemotherapeutic drugs passively and more specifically to tumor sites, thereby limiting any damage to healthy tissues (9,10). A number of recent experimental (3,7,11–17) and theoretical (18–23) studies have suggested that particles of certain sizes and shapes have a higher margination propensity. This would facilitate the diffusion of these particles into tumor sites by allowing them to reach the leaky blood vessel walls and, ultimately, the tumors. Understanding the distribution of particles in blood flow is vital for the rational design of drug-carrying particles for cancer therapy. Such an understanding may also impact the application of particles for bioimaging applications, where a low or no margination propensity would help increase the particle circulation time (24). Further, the margination of particles has been successfully exploited to separate cells (e.g., sickle cells) and pathogens (e.g., bacteria and fungi) according to their size and/or stiffness (25–28).

The current understanding of margination is that two driving forces contribute to it, namely, wall-induced lift forces and heterogeneous collisions between red blood cells (RBCs), WBCs, and particles. Lift forces arise from an asymmetric pressure field that develops as the particle deforms near the wall, which consequently pushes cells or particles away from the wall (29,30). The magnitude of the lift force depends on the deformability of the cells or particles.

Submitted March 9, 2016, and accepted for publication August 22, 2016.

*Correspondence: anson.ma@uconn.edu

Editor: Charles Wolgemuth.

http://dx.doi.org/10.1016/j.bpj.2016.08.026

RBCs are less stiff than WBCs and as a result, the lift forces experienced by RBCs are larger, leading to the formation of a layer free of RBCs, known as the cell-free layer (CFL), as shown in Fig. 1 *a* (31–33). Further, particle dynamics simulations by Kumar and Graham (34) and Kumar et al. (35) revealed that collisions between stiff and floppy particles in a suspension resulted in the eventual movement of stiff particles toward the wall. Collisions in the near-wall region between stiff and floppy particles resulted in a greater displacement of the stiff particles toward the wall, and margination did not occur in cases where only one particle type was present (34,35). It follows that once a stiff particle reaches the near-wall CFL, it tends to remain there (34,35). This phenomenon in combination with the CFL, which arises from lift forces, is thought to be responsible for the margination of particles in blood flow (32). Further, the migration velocities and collision tendencies of particles have been linked with margination behavior (36).

A number of experimental (3,7,11–17) and theoretical (19,21–23) studies have explored the effect of varying particle size on the margination propensity of particles. Several studies suggested that larger particles marginate much more readily than smaller particles, and that there is an optimal particle size for margination (3,12,14,15,19,22,23). There is, however, no consensus as to the exact particle size that results in optimal margination. With regard to the effect of flow rate, Charoenphol et al. (12) experimentally observed that margination increased with an increasing flow rate.

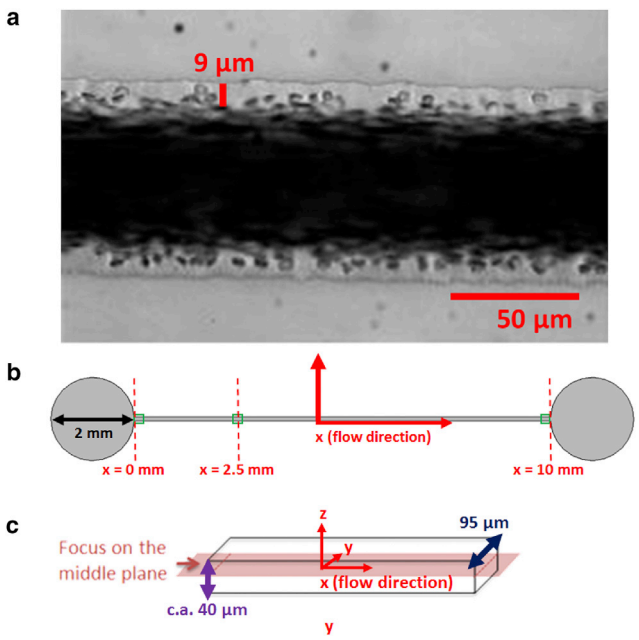

FIGURE 1 (*a*) Blood flow showing the formation of CFL within a microchannel. (*b*) Plane of focus for particle tracking with labeled imaging positions. (*c*) Schematic diagram of the microfluidic channel used in this study with the plane of focus for particle tracking. To see this figure in color, go online.

However, for a given particle concentration and duration, a larger total number of particles would perfuse through the device at higher flow rates, which may explain the trend they observed. Interestingly, a later independent experimental study by Namdee et al. (3) suggested that margination decreased with increasing flow rate, contradicting the study by Charoenphol et al. (12). Namdee et al. (3) attributed this to the measurement method they used, which involves perfusing a suspension of fluorescent particles through a microfluidic channel, flushing with a buffer solution, and measuring the fluorescence intensity emitted by particles that remain adhered to the wall. Particles may have detached from the wall at higher flow rates due to increasing hydrodynamic drag and/or collision with RBCs (3). In addition to particle size and flow rate, margination also depends on other factors such as particle shape, density, and stiffness, as well as blood hematocrit (10). Detailed reviews on margination and the effects of each of these factors are available (10,37).

In this study, we focus on how the suspending medium, particle size, and flow rate affect the margination propensity. This work differs from previous studies in a number of ways. First, all previous experimental studies, with only two exceptions (7,38), assessed margination propensity based on the number density, or, more precisely, the fluorescence intensity, of fluorescent particles that adhered to the channel wall after a particle suspension and subsequently a buffer solution passed through the channel (3,11–14,16–18,39). Although adhesion is related to margination, adhesion also depends on other factors such as hydrodynamic drag, the densities of ligands and receptors grafted onto the particle surface and the wall channel, the particle shape and contact orientation, and the particle size relative to the CFL (10,16,17,20,21). In this work, the margination propensity was quantified based on the direct tracking of individual particles. Direct tracking is less susceptible to the aforementioned factors, which further complicate the interpretation of experimental results. Instead of manually tracking a limited number of particles, we developed a numerical code to track thousands of particles and ensure that the experimental results reported herein would be statistically significant (see Supporting Materials and Methods in the Supporting Material). Second, individual particles were experimentally tracked to calculate the velocities both in the flow direction and in the margination direction. Mean-square displacement data were further used to estimate the effective particle diffusivities in water and blood, respectively. Third, the degrees of margination at different travel distances from the inlet were assessed experimentally and analyzed.

MATERIALS AND METHODS

Materials

Defibrinated bovine blood (Lampire Biological Laboratories, Pipersville, PA) was washed and adjusted to 35% hematocrit. Briefly, the bovine blood

was first centrifuged at 500 × *g* and the plasma was decanted. Phosphate-buffered saline (Thermo Fisher Scientific, Waltham, MA) was added to the blood to adjust it to a physiologically relevant 35% hematocrit (40,41). This process was repeated twice to ensure a thorough washing. Although this process may have removed bovine serum albumin and other proteins that are naturally present in blood plasma, it minimized particle adhesion in the channel. In unwashed blood, such particle adhesion to the bottom of the channel made particle tracking difficult or impossible (see Supporting Materials and Methods). Furthermore, the washing of bovine blood and its resuspension in phosphate-buffered saline resulted in bovine RBCs with elasticities similar to those of human RBCs (42). Spherical, fluorescent polystyrene particles (0.53, 0.84, and 2.11 μm in diameter) were used as model particles in the experimental system (Spherotech, Lake Forest, IL). These particle sizes were chosen because the endothelial cell spacing of leaky vasculature near tumor sites typically varies from 0.2 μm to 2 μm (43); 2.11 μm was chosen as the largest particle size. A smaller particle size (0.25 μm) was tested initially, but accurate tracking of particle positions at the mid-plane was impossible due to the limited fluorescence signal and the obstruction of RBCs. Therefore, 0.53 μm was chosen as the smallest particle size in this study. The original number concentrations of particles were 1.22×10^{11}, 3.07×10^{10}, and 1.94×10^{9} particles/mL for 0.53-, 0.84-, and 2.11-μm particles, respectively. A polydimethylsiloxane (PDMS) prepolymer and curing agent were used for the fabrication of microfluidic devices (Silgard 184 Silicone Elastomer Kit; Krayden, Denver, CO).

Microfluidic device fabrication

A conventional soft lithography technique using SU-8 photoresist (Thermo Fisher Scientific) was used to fabricate a silicon master. Briefly, SU-8 2025 photoresist (MicroChem, Newton, MA) was spin-coated onto a 3" silicon wafer (NOVA Electronic Materials, Flower Mound, TX), exposed to UV light through a transparency photomask (Advanced Reproductions, North Andover, MA) designed using AutoCAD software, and submerged in developer solution (MicroChem). Upon drying, microfluidic devices were fabricated from the silicon master using PDMS (Silgard 184 Silicone Elastomer Kit; Krayden). The elastomer base and curing agent were mixed in a 10:1 ratio and degassed for 10 min. Next, the PDMS was poured over the master and degassed for an additional 10 min. The master was placed in an oven and the PDMS was allowed to cure for 2 h at 60°C. The device was cut out with a scalpel, and an inlet and outlet were created by using a 2-mm biopsy punch (Miltex, York, PA) and punching vertically through the PDMS into the 2-mm landing pad area of the device, as shown in Fig. 1 *b*. Lastly, the PDMS device was plasma bonded (Basic Plasma Cleaner PDC-32G; Harrick Plasma, Ithaca, NY) to a glass coverslip slide (#1.5; Thermo Fisher Scientific) to form a completed microfluidic device.

Experimental setup

Spherical, fluorescent polystyrene particles (0.53, 0.84, and 2.11 μm in diameter; Spherotech) were diluted in the washed bovine blood and in water such that the final number concentration was calculated to be 4.073×10^{6} particles/mL. A pressure-driven pump system with a flow controller (Fluigent, Villejuif, France) was used to pump each solution through the microfluidic device at a physiologically relevant average velocity of 1 mm/s (44–47). This velocity corresponds to a volumetric flow rate of 0.24 μL/min and an apparent wall shear rate of 61 s^{-1} for our channel dimensions. The apparent wall shear rates depend on the volumetric flow rates as well as the channel dimensions, but do not account for the non-Newtonian nature of blood or the formation of the CFL. For a rectangular channel with a width w and a depth d, the apparent wall shear rate is calculated as $(6Q/WH^2)(1+(H/W))f^*(H/W)$, where H is the channel height, W is the channel width, Q is the volumetric flow rate, and f^* is a geometric constant based on the ratio of H and W (48). The pressure-driven pump system provides better control of the flow rate than a syringe pump (see Supporting Materials and Methods). A number of 60,000-frame (~7.5 min) time-lapse videos of the flowing suspensions were acquired at the middle plane of the microfluidic device, as shown in Fig. 1 *c*, using a dry objective lens (40×) with a high-speed camera (Andor iXon Ultra 897 iX0897 EMCCD, 130 frames/s; Andor Technology Ltd., Belfast, UK) and an inverted fluorescence microscope (Nikon Eclipse Ti-E, Nikon Instruments, Melville, NY) with an epifluorescence source (Intensilight C-HGFIE; Nikon Instruments). After each time-lapse video was collected, the reservoir of blood was gently shaken to keep the solution well mixed and the device was perfused at a high flow rate (~8 μL/min) for ~2 min. After every four time lapses, the entire system was flushed for 10 min before the next time-lapse video was taken.

Image analysis: particle tracking

The collected time-lapse videos were analyzed using MATLAB (The MathWorks, Natick, MA) code developed in-house. Briefly, the tracking consisted of three steps. First, a background correction was performed to remove any bright pixels associated with particles that adhered to the bottom of the channel. Second, the position and size of all particles were calculated using a gradient-based method. The calculated particle size was used to eliminate out-of-focus particles based on their apparent larger size. Third, the positions of all remaining particles were tracked as a function of time to calculate displacements and velocities. A more in-depth explanation of the image analysis is given in Supporting Materials and Methods.

RESULTS AND DISCUSSION

Quantifying the margination propensity

Fig. 2, *a* and *b*, show the number of particles that were tracked as a function of the normalized y-position in water and blood, respectively. The Reynolds number was calculated to be ~0.018, suggesting that viscous forces were dominant in relation to the inertial forces and that the flow was laminar. In each case, a higher particle count was recorded close to the centerline. This can be explained by the velocity profile for pressure-driven flow through the channel, where the velocity is higher closer to the centerline. Fig. 2, *c* and *d*, show the actual velocity profiles (x-direction) obtained by tracking the velocity of individual particles in water and blood, respectively. A parabolic velocity profile was recorded in the water case, as expected for a simple Newtonian fluid, whereas the blood case showed a profile closer to that of a plug flow. The formation of a CFL and the higher concentration of RBCs near the centerline likely contributed to this profile. Such a blunted plug-flow velocity profile for blood was first observed experimentally by Goldsmith and Spain (31). Higher velocities near the centerline will naturally lead to a higher particle count since more particles are transported through the channel in a given time, for a uniform dispersion. To correct for the actual velocity profiles, the particle count was weighted according to the particle velocities:

$$P_{i^{th}\,segment\in[1,10]} = \sum_{j\in[1,n]} \frac{v_{x,max}}{v_{x,j}}, \qquad (1)$$

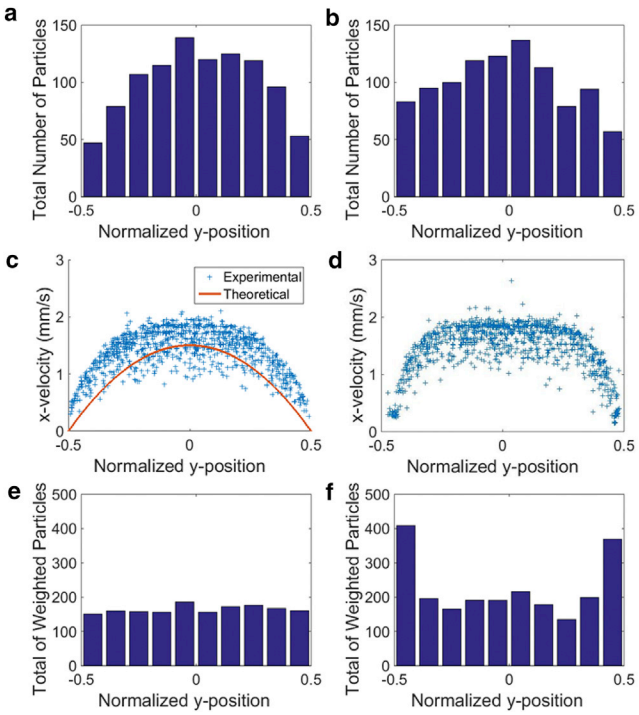

FIGURE 2 (*a* and *b*) Particle count per segment as a function of the normalized y-position for 2.11-μm particles suspended in (*a*) water and (*b*) blood. Volumetric flow rate: 0.24 μL/min; apparent wall shear rate: 61 s^{-1}. (*c* and *d*) Velocity profiles of 2.11-μm particles suspended in (*c*) water and (*d*) blood. (*e* and *f*) Total weighted particle count per segment ($P_{i^{th}segment}$) as a function of the normalized y-position for (*e*) water and (*f*) blood. To see this figure in color, go online.

where $P_{i^{th}segment}$ is the total weighted particle count for the i^{th} segment, $v_{x,max}$ is the maximum particle velocity across the channel, $v_{x,j}$ is the velocity of the j^{th} particle within the i^{th} segment, and n is the total number of particles within the i^{th} segment. Effectively, each particle in a given segment is assigned a weighted value. Equation 1 is set up to correct for the intrinsic velocity profile, where particles found closer to the wall always move at a lower velocity and, consequently, fewer particles are recorded closer to the wall relative to the center. Using Eq. 1, particles moving at a slower speed will be weighted more than fast-moving particles. For instance, for a $v_{x,max}$ of 1 mm/s, a particle moving at 0.1 mm/s near the wall will have a weighted value of 10, whereas a particle moving at 0.9 mm/s near the center will have a weighted value of 1.11. Further, this method also corrects for any difference in the actual velocity profile under different experimental conditions, such as suspending medium and wall shear rates. The use of this method is further supported by Fig. 2, *e* and *f*, which show the weighted particle counts for different segments across the channel for water and blood, respectively. In the case of water, no preferential accumulation in the near-wall segments was observed, whereas the blood case clearly showed higher weighted particle counts in the segments nearest to the walls. Such trends are not so apparent in the original particle counts before velocity profile correction (i.e., Fig. 2, *a* and *b*).

There are several definitions for margination propensity in the literature. In adhesion studies, the fluorescence intensity of adhered particles is directly correlated with the number of particles that marginate. The higher the fluorescence intensity, the higher the margination propensity. In simulation studies, where the exact center of mass of particles is known, margination is conveniently defined as the number of particles at a given characteristic distance from the wall (e.g., the CFL thickness or adhesion distance) (15,20,21,23,37,49). In this study, each segment width was ~9.5 μm, which is close to the CFL thickness, as shown in Fig. 1 *a* and in Movies S1, S2, S3, S4, and S5. Thus, we define the margination parameter, M, as

$$M = \frac{P_{1^{st}segment} + P_{10^{th}segment}}{\sum_{i^{th}segment \in [1,10]} P_i}. \quad (2)$$

With a total of 10 segments and the fact that two of the segments are close to the wall, if there is no margination and an even distribution of particles, then M should be equal to 0.2, as 20% of the total number of particles should be found near the channel sidewalls. M is, fundamentally, the percentage of particles that are in the CFL after weighting and thus have marginated (as defined in this study). An M-value of 0.2 or 20% is equivalent to an even distribution of particles and is expected for the control experiments using water. Fig. 2 *e* shows a typical plot for a water experiment. Each segment has an approximately equal total weighted particle count and the M-value of this plot is ~0.20, as expected for a water experiment. Values that are higher than this indicate marginating behavior. As shown in Fig. 2 *f*, with blood as the suspending medium, segments 1 and 10 have higher total weighted particle counts compared with the rest of the channel. In fact, this particular plot has an M-value of ~0.33, suggesting margination. For each experimental condition, a total of 3000 particles were analyzed to ensure that the results would be statistically significant (see Supporting Materials and Methods). The average and standard deviation of the margination parameter, M, was calculated based on every 1000 particles tracked.

Effect of suspending medium: water versus blood

Fig. 3 *a* shows M as a function of x (see Fig. 1 *b*), the distance from the inlet, for three different particle sizes (0.53 μm, 0.84 μm, and 2.11 μm) in water. At the channel inlet ($x = 0$ mm) in water, all three particle sizes showed an M-value close to 0.2, indicating that the particles were evenly distributed after velocity gradient correction and that there was no margination. The M-value at $x = 10$ mm in water was also calculated for each particle size studied.

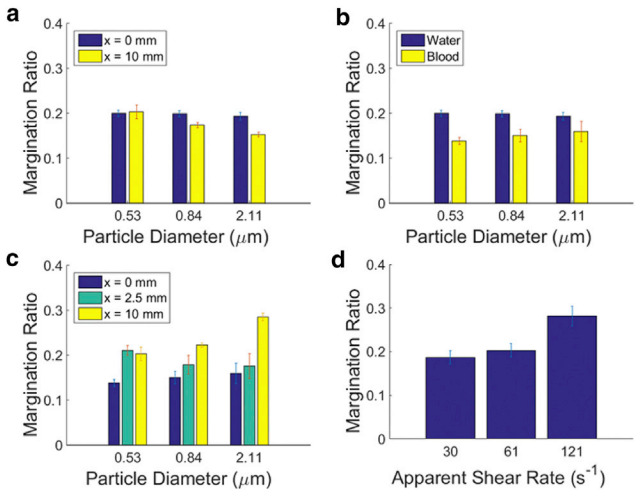

FIGURE 3 (*a–c*) Margination parameter (*M*) for different sizes of particles: (*a*) suspended in water at the inlet ($x = 0$) and outlet ($x = 10$ mm), (*b*) suspended in water or blood at $x = 0$, and (*c*) suspended in blood at different channel positions (x). For (*a–c*), apparent wall shear rate = 61 s^{-1}. (*d*) Margination parameter (*M*) of 0.53-μm particles suspended in blood at varying flow rates at the outlet ($x = 10$ mm). To see this figure in color, go online.

Interestingly, both the 0.84-μm and 2.11-μm particles showed an *M*-value lower than 0.2. This may be explained by sedimentation, where settling velocities are dependent on particle size to the second power. Using the Stokes-Einstein equation (50) ($\mathrm{Re} = 0.018 << 1$), the settling velocities were estimated to be 0.459 μm/min, 1.15 μm/min, and 7.27 μm/min for the 0.53-μm, 0.84-μm, and 2.11-μm particles. Given the parabolic velocity profile, particles close to the wall were traveling at a significantly slower speed relative to particles near the centerline, and thus particles closer to the wall had a longer residence time and were more prone to sedimentation. As only the middle plane ($z \approx 0$) was imaged, settling particles became out of focus and therefore were not recorded by the particle-tracking code. Although the density of the medium may be matched with that of the particle to mitigate the effects of sedimentation, such an approach was not pursued in this study because such density differences may also exist for actual drug carriers, and possible sedimentation effects should be considered.

The distance required to establish a fully developed flow in a microfluidic device is estimated to be 52.2 μm for water using the following equation and a calculated Reynolds number of 0.018 for the experiment presented here (51):

$$\frac{x_e}{L_c} = \frac{0.55}{0.13\mathrm{Re} + 1} + 0.065\mathrm{Re}, \qquad (3)$$

where x_e is the entrance length from the inlet that is required in order for flow to be considered fully developed, and L_c is the characteristic length, or the width of the channel (95 μm). Equation 3 assumes the fluid is a homogeneous Newtonian fluid, which is valid for water, but not for blood. Fig. 3 *b* compares the *M*-value of three different sizes of particles at the inlet (i.e., $x = 0$) where the particles were suspended in water and blood. For all particle sizes studied, the *M*-value was lower for blood than for water, suggesting that fewer particles were found close to the channel wall at the entrance in blood. However, as shown in Fig. 3 *c*, the *M*-values downstream at $x = 2.5$ mm have returned to those observed in water (~0.2). We hypothesize that the reduction in *M*-value at the entrance is associated with an entrance flow effect as the blood-particle suspension is perfused through the tubing into the 2-mm-diameter inlet and the microfluidic channel (Fig. 1 *b*). Blood is a non-Newtonian fluid and the flow is heterogeneous, so the distance required to establish a fully developed flow is likely to be greater for blood than for water. Indeed, as predicted by simulations by Katanov et al. (52), the distance required for the CFL to fully develop is on the order of 2.4 mm for our microchannel, further supporting the experimental observations of this study. Furthermore, this experimental observation has two important implications. First, it implies that the usual, implicit assumption about a uniform dispersion of particles at the entrance of a microfluidic device or other experimental system may not be true. Second, although the presence of a flow constriction is not a requirement for margination to occur, it may have a nonnegligible effect on particle margination. Since most microfluidic devices feature a constriction where fluid enters the channel from a larger inlet punch, results could be affected. It is therefore important to collect data not only at a downstream channel location but also near the inlet to ensure an accurate interpretation of the results. Although the exact effect of flow constrictions is beyond the original scope of this work, this experimental observation has important implications for drug delivery in vascular networks, where many different geometries and constriction shapes are possible. The potential effects of constriction geometry on margination may be significant and warrant further investigation in a future study.

Margination velocity and effective diffusivity

Direct tracking of particles enables the analysis of velocity not only in the flow direction (x) but also across the channel width (y-direction), which is of direct relevance to margination. In fact, margination velocities and the corresponding standard deviations were reported in previous simulation studies (34,53) in which the exact particle positions were known. However, no other previous experimental studies have reported these values. Fig. 4, *a–f*, show the y-velocity (v_y), or margination velocity, of individual particles as calculated from direct particle tracking in water and blood, respectively. It should be noted that these v_y-values are averaged per particle and that a positive v_y corresponds to the movement of a particle toward either wall of the channel,

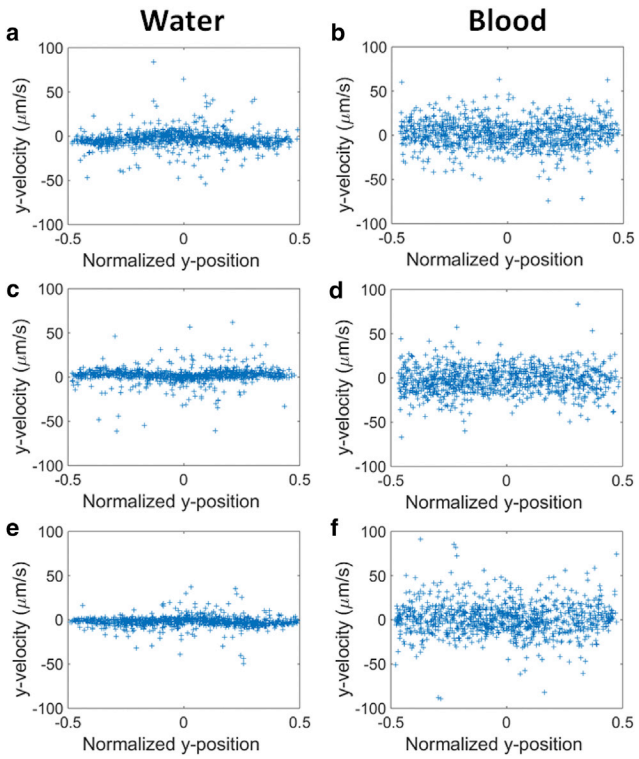

FIGURE 4 (*a–f*) Representative plots of average y-velocities for individual particles in water or blood: (*a* and *b*) 0.53-μm, (*c* and *d*) 0.84-μm, and (*e* and *f*) 2.11-μm particles. To see this figure in color, go online.

whereas a negative v_y indicates that a particle is moving toward the center of the channel. The v_y is calculated from the center of mass of the particle based on the brightness of the pixels. Briefly, we first weight each pixel by its relative brightness and then find the center of mass by finding the center of brightness. This gives us the center of the particle with a subpixel resolution, and we can then calculate the y-velocity of the particle from frame to frame. In fact, the relatively large size of any blurred particle image provides more pixels for calculating the center of the particle and increases the precision of calculating the position. For all particle sizes studied, there is a larger spread in v_y in blood compared with water as the suspending medium. The standard deviation in v_y, denoted as v_y', was calculated to be on the order of 9 μm/s for water (averaged over all three particle sizes) versus ~16 μm/s for blood, as shown in Table 1. The larger v_y'-value in the blood case is attributed to collisions between particles and blood cells, which are absent in the water case. However, no noticeable difference in v_y'-values was observed among the different particle sizes, probably because of the relatively short travel distance in the y-direction, as limited by the field of view (205 × 205 μm). Further, we estimated the translational diffusivities of particles in water and blood by plotting the mean-square displacement as a function of time, as shown in Fig. 5, *a* and *b*, and calculating the slope (*s*), where $D_y = s/2$. A relatively large error arises from the spatial and temporal limitations of our imaging

TABLE 1 Experimental Diffusivities and Standard Deviations of v_y versus Particle Size

	v_y' (μm/s)		Experimental Diffusivity (μm²/s)	
Size (μm)	Water	Blood	Water	Blood
0.53	9.30 ± 0.23	15.44 ± 1.45	4.91 ± 0.78	14.20 ± 1.96
0.84	9.34 ± 0.70	16.16 ± 0.80	4.40 ± 0.17	14.87 ± 2.34
2.11	7.10 ± 1.44	17.48 ± 0.74	1.88 ± 0.14	15.42 ± 1.15

system. Also, RBCs can obscure some of the fluorescent signal of the particles. Despite the relatively large error in determining the particle position at short timescales, the calculated values for the water cases are of the same order of magnitude as the Brownian diffusivities calculated using the Stokes-Einstein-Sutherland equation (54). As expected, the smaller the particle size, the higher the diffusivity in water. The higher experimental values may be caused by shear-induced diffusion (55). In the blood cases, the effective diffusivities are all on the order of 15 μm²/s, which is much higher than those measured for the water cases (on the order of 2–5 μm²/s), as shown in Table 1. As in the case with v_y', this is probably caused by the collisions between particles and blood cells. Interestingly, in blood, the larger the particle size, the higher the effective diffusivity, suggesting that collisions, rather than Brownian motions, are a predominant factor for margination.

Effect of particle size

Using the *M*-values at $x = 2.5$ mm as benchmarks, the 2.11-μm particles showed the largest change in *M*-value and thus the highest margination propensity, with a 45% increase relative to the case of an even distribution of particles, followed by the 0.84-μm particles and the 0.53-μm particles. Therefore, larger particle sizes were found to result in a higher margination propensity. The 0.53-μm particles showed similar *M*-values close to 0.2 at $x = 2.5$ mm and 10 mm, suggesting there is no margination for this particle

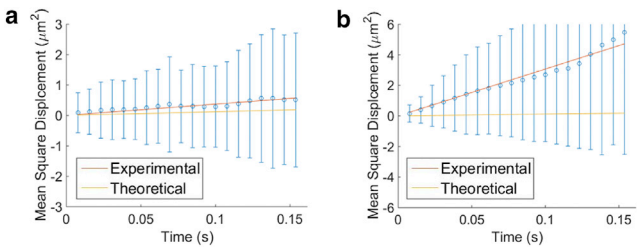

FIGURE 5 (*a* and *b*) Mean-square displacement as a function of time for 2.11-μm particles in (*a*) water and (*b*) blood. Theoretical lines (*yellow*) on both plots have a slope equal to two times the Brownian diffusivity, which is calculated to be ~0.6 μm²/s using the Stokes-Einstein-Sutherland equation. From data fitting, the effective diffusivities were estimated to be ~1.9 μm²/s and ~15.4 μm²/s for water and blood, respectively. To see this figure in color, go online.

size once the flow is fully established. This is in agreement with the findings from adhesion studies (3,11–14,17,18), as well as a recent direct-particle-tracking study by D'Apolito et al. (7) in which two spherical particle sizes (1 μm and 3 μm) were investigated. It is conjectured that larger particles interact more readily with RBCs and, as a result of their frequent collisions with RBCs, are propelled toward the walls of a blood vessel sooner than smaller particles, which have less frequent interactions. Zhao et al. (56) put forward an equation to calculate the distance required for a particle to reach the CFL, or the margination distance:

$$X = \frac{\langle u \rangle \left(\frac{w}{4}\right)^2}{D_y}, \tag{4}$$

where $\langle u \rangle$ is the average flow-direction velocity, w is the channel width, and D_y is the diffusivity in the y-direction. Using the effective diffusivities estimated experimentally (see above), the margination distance is calculated from Eq. 4 to be on the order of 7.5 mm. Since the M-values are close to 0.2 at $x = 2.5$ mm, the M-values at $x = 10$ mm likely reflect completed margination.

Effect of flow rate

As discussed in the Introduction, studies using particle adhesion to assess margination have reported two opposite trends for the effect of flow rates (3,12). Although adhesion and margination are related, evaluating margination based on the number of adhered particles could be further complicated by factors such as hydrodynamic drag, the densities of ligands and receptors grafted onto both the particle surface and the wall channel, the particle shape and contact orientation, and the particle size relative to the CFL (10,20,21). Particles may have detached from the wall due to collisions with blood cells or increasing wall shear rate. This may explain why the margination propensity decreases as a function of increasing flow rate (3). Further, only particles that come into direct contact with the wall are being measured. This method does not account for particles that marginate to the CFL but do not adhere to the wall. As a result, larger particles may be predisposed to adhere more readily due to their larger size relative to the CFL. In this study, the margination parameter (M) was calculated based on the actual velocity profile and normalized by the total number of particles that perfused through the microchannel for a given time. This analysis method is less susceptible to any variation in the actual particle number concentration. It also offers a fairer comparison of different flow rates because the total number of particles that perfuse through the device increases as a function of increasing flow rates (for a given number concentration and perfusion time). As shown in Fig. 3 *d*, the higher the flow rate, the higher the M-value. This is probably caused by higher collision frequencies between particles at higher flow rates. This explanation is consistent with the observation that the standard deviation of particle velocity in the y-direction (v_y) increases as a function of increasing flow rates, as shown in Table 2.

CONCLUSIONS

To summarize, the margination of particles in blood was characterized by directly tracking the spatial distribution of particles passing through a microfluidic channel at different physiologically relevant flow rates. A margination parameter, M, was defined to quantify the margination propensity after correcting for the velocity gradient in the flow direction (x). A benchmark value of 0.2 was established through a control experiment in which the particles were suspended in water with no margination. When suspended in water, particles that were close to the channel wall and had longer residence times due to the velocity profile in the channel tended to settle, leading to relatively fewer particles near the wall at the outlet ($x = 10$ mm) and consequently an M-value of <0.2 for the 0.84-μm and 2.11-μm particles. The M-values for all particle sizes at the entrance ($x = 0$) were smaller for particles suspended in blood compared with those in water. This is probably due to non-fully-developed flow and constriction as the blood-particle mixture entered from the tubing and inlet into the microfluidic channel. The largest particles (2.11 μm) showed the highest margination propensity near the outlet in blood ($x = 10$ mm), followed by the 0.84-μm particles, whereas the 0.53-μm particles showed no margination. Although the results cannot be compared directly with other studies because of differences in experimental conditions, the observed trend is qualitatively consistent with results reported by earlier experimental and simulation studies.

In addition to M, the particle velocity in the margination direction (v_y) was characterized experimentally for the first time, to our knowledge. Compared with the case of water, all particle sizes showed a larger fluctuation in v_y when suspended in blood. Likewise, a higher effective diffusivity, on the order of 15 $\mu m^2/s$, was also observed in all of the blood cases relative to the water cases, which varied from 2–5 $\mu m^2/s$. The larger fluctuations in v_y and higher effective diffusivity in blood are probably caused by the collisions between particles and blood cells, consistent with arguments put forward in earlier simulation studies (20,35,37,53). Further, the calculation of M accounts for the actual velocity

TABLE 2 Standard Deviation of v_y (v_y') for Varying Flow Rates in Blood

Apparent Wall Shear Rate (s^{-1})	v_y' (μm/s)
30	10.27
61	14.22
121	23.68

gradient and the absolute total number of particles that pass through the channel, offering a more robust way to compare data collected at different flow rates. An increase in flow rate led to both a larger M-value at the exit and a higher effective diffusivity, confirming experimental results reported by Charoenphol et al. (12). However, this study does have several limitations. First, particle tracking is limited by the spatial and temporal resolution of the imaging system, the relatively small field of view, and the presence of RBCs, which at higher hematocrits can absorb and scatter light and make the direct tracking of fluorescent particles challenging. No significant difference in terms of the margination velocity and diffusivity was observed among different-sized particles suspended in blood. Second, this study focuses on the distribution of particles within the channel and does not account for the transport of particles through the spacing between endothelial cells, which typically varies from 0.3 to 4.7 μm (57). Large particles may exhibit a greater margination propensity but may not be small enough to pass through the spacing to reach the tumor site. Finally, according to Wiedeman (58), the length of an arteriole in vivo is only ~1 mm, with branches of other arteries every 0.2 mm, so the length scale is not as close to the in vivo situation as it could be. In summary, in this work we investigated the effects of particle size and shear rate on margination propensity based on the particle distribution, velocity (both along and transverse to the flow direction), and effective diffusivity. The findings suggest that margination is primarily caused by collisions between particles and blood cells, rather than by Brownian motion.

SUPPORTING MATERIAL

Supporting Materials and Methods, two figures, one table, and five movies are available at http://www.biophysj.org/biophysj/supplemental/S0006-3495(16)30748-2.

AUTHOR CONTRIBUTIONS

E.J.C. contributed to designing the research, performing the research, developing analytical tools, analyzing data, and writing the manuscript. B.H.B. contributed to developing analytical tools and writing the manuscript. G.M.B., A.L.K., and L.M.S. all contributed their expertise regarding fabrication techniques for the microfluidic devices used in this study. M.D.W. contributed to analyzing early data. A.W.K.M. contributed to designing the research, analyzing the data, and writing the manuscript.

ACKNOWLEDGMENTS

The authors thank Prof. Henning Winter (University of Massachusetts Amherst) and Prof. Suzy Torti (University of Connecticut Health Center) for useful discussions, Dr. Carol Norris (University of Connecticut) for microscopy training, and Prof. Craig Nelson's group (University of Connecticut) for blood-washing training.

This material is based on work supported by a National Science Foundation Graduate Research Fellowship under grant No. DGE-1247393, the National Science Foundation under grant No. 1250661, and the Department of Defense Mentor-Predoctoral Fellow Research Award Program under award No. W81XWH-10-1-0434.

REFERENCES

1. Dutrochet, H. 1824. Recherches Anatomiques et Physiologiques sur la Structure Intime des Animaux et des Végétaux, et sur Leur Motilité. J. B. Baillière, Paris.
2. Segré, G., and A. Silberberg. 1962. Behaviour of macroscopic rigid spheres in Poiseuille flow. Part 2. Experimental results and interpretation. *J. Fluid Mech.* 14:136–157.
3. Namdee, K., A. J. Thompson, …, O. Eniola-Adefeso. 2013. Margination propensity of vascular-targeted spheres from blood flow in a microfluidic model of human microvessels. *Langmuir.* 29:2530–2535.
4. Suzuki, R., D. Omata, …, K. Maruyama. 2016. Cancer therapy with nanotechnology-based drug delivery systems: applications and challenges of liposome technologies for advanced cancer therapy. *In* Methods in Pharmacology and Toxicology. Springer, New York, pp. 457–480.
5. Kanapathipillai, M., A. Brock, and D. E. Ingber. 2014. Nanoparticle targeting of anti-cancer drugs that alter intracellular signaling or influence the tumor microenvironment. *Adv. Drug Deliv. Rev.* 79-80:107–118.
6. Sakurai, Y., K. Kajimoto, …, H. Harashima. 2015. Advances in an active and passive targeting to tumor and adipose tissues. *Expert Opin. Drug Deliv.* 12:41–52.
7. D'Apolito, R., G. Tomaiuolo, …, S. Guido. 2015. Red blood cells affect the margination of microparticles in synthetic microcapillaries and intravital microcirculation as a function of their size and shape. *J. Control. Release.* 217:263–272.
8. Matsumura, Y., and H. Maeda. 1986. A new concept for macromolecular therapeutics in cancer chemotherapy: mechanism of tumoritropic accumulation of proteins and the antitumor agent smancs. *Cancer Res.* 46:6387–6392.
9. Decuzzi, P., R. Pasqualini, …, M. Ferrari. 2009. Intravascular delivery of particulate systems: does geometry really matter? *Pharm. Res.* 26:235–243.
10. Carboni, E., K. Tschudi, …, A. W. Ma. 2014. Particle margination and its implications on intravenous anticancer drug delivery. *AAPS PharmSciTech.* 15:762–771.
11. Doshi, N., B. Prabhakarpandian, …, S. Mitragotri. 2010. Flow and adhesion of drug carriers in blood vessels depend on their shape: a study using model synthetic microvascular networks. *J. Control. Release.* 146:196–200.
12. Charoenphol, P., R. B. Huang, and O. Eniola-Adefeso. 2010. Potential role of size and hemodynamics in the efficacy of vascular-targeted spherical drug carriers. *Biomaterials.* 31:1392–1402.
13. Gentile, F., C. Chiappini, …, P. Decuzzi. 2008. The effect of shape on the margination dynamics of non-neutrally buoyant particles in two-dimensional shear flows. *J. Biomech.* 41:2312–2318.
14. Gentile, F., A. Curcio, …, P. Decuzzi. 2008. The margination propensity of spherical particles for vascular targeting in the microcirculation. *J. Nanobiotechnology.* 6:9.
15. Lee, T. R., M. Choi, …, P. Decuzzi. 2013. On the near-wall accumulation of injectable particles in the microcirculation: smaller is not better. *Sci. Rep.* 3:2079.
16. Toy, R., E. Hayden, …, E. Karathanasis. 2011. The effects of particle size, density and shape on margination of nanoparticles in microcirculation. *Nanotechnology.* 22:115101.
17. Decuzzi, P., F. Gentile, …, M. Ferrari. 2007. Flow chamber analysis of size effects in the adhesion of spherical particles. *Int. J. Nanomedicine.* 2:689–696.

18. Tan, J., S. Shah, …, Y. Liu. 2013. The influence of size, shape and vessel geometry on nanoparticle distribution. *Microfluid. Nanofluidics.* 14:77–87.

19. Decuzzi, P., S. Lee, …, M. Ferrari. 2005. A theoretical model for the margination of particles within blood vessels. *Ann. Biomed. Eng.* 33:179–190.

20. Vahidkhah, K., and P. Bagchi. 2015. Microparticle shape effects on margination, near-wall dynamics and adhesion in a three-dimensional simulation of red blood cell suspension. *Soft Matter.* 11:2097–2109.

21. Müller, K., D. A. Fedosov, and G. Gompper. 2014. Margination of micro- and nano-particles in blood flow and its effect on drug delivery. *Sci. Rep.* 4:4871.

22. Lee, S. Y., M. Ferrari, and P. Decuzzi. 2009. Shaping nano-/micro-particles for enhanced vascular interaction in laminar flows. *Nanotechnology.* 20:495101.

23. Müller, K., D. A. Fedosov, and G. Gompper. 2016. Understanding particle margination in blood flow - A step toward optimized drug delivery systems. *Med. Eng. Phys.* 38:2–10.

24. Godin, B., R. E. Serda, …, M. Ferrari. 2010. Nanoparticles for cancer detection and therapy. *In* Nanotechnology. Wiley-VCH, Weinheim, Germany.

25. Munn, L. L., and M. M. Dupin. 2008. Blood cell interactions and segregation in flow. *Ann. Biomed. Eng.* 36:534–544.

26. Jain, A., and L. L. Munn. 2011. Biomimetic postcapillary expansions for enhancing rare blood cell separation on a microfluidic chip. *Lab Chip.* 11:2941–2947.

27. Hou, H. W., A. A. S. Bhagat, …, C. T. Lim. 2010. Deformability based cell margination—a simple microfluidic design for malaria-infected erythrocyte separation. *Lab Chip.* 10:2605–2613.

28. Wei Hou, H., H. Y. Gan, …, J. Han. 2012. A microfluidics approach towards high-throughput pathogen removal from blood using margination. *Biomicrofluidics.* 6:24115.

29. Abkarian, M., C. Lartigue, and A. Viallat. 2002. Tank treading and unbinding of deformable vesicles in shear flow: determination of the lift force. *Phys. Rev. Lett.* 88:068103.

30. Abkarian, M., and A. Viallat. 2005. Dynamics of vesicles in a wall-bounded shear flow. *Biophys. J.* 89:1055–1066.

31. Goldsmith, H. L., and S. Spain. 1984. Margination of leukocytes in blood flow through small tubes. *Microvasc. Res.* 27:204–222.

32. Narsimhan, V., H. Zhao, and E. S. G. Shaqfeh. 2013. Coarse-grained theory to predict the concentration distribution of red blood cells in wall-bounded Couette flow at zero Reynolds number. *Phys. Fluids.* 25:061901.

33. Lim, E. J., T. J. Ober, …, M. Toner. 2012. Visualization of microscale particle focusing in diluted and whole blood using particle trajectory analysis. *Lab Chip.* 12:2199–2210.

34. Kumar, A., and M. D. Graham. 2011. Segregation by membrane rigidity in flowing binary suspensions of elastic capsules. *Phys. Rev. E Stat. Nonlin. Soft Matter Phys.* 84:066316.

35. Kumar, A., R. G. Henríquez Rivera, and M. D. Graham. 2014. Flow-induced segregation in confined multicomponent suspensions: effects of particle size and rigidity. *J. Fluid Mech.* 738:423–462.

36. Henríquez Rivera, R. G., K. Sinha, and M. D. Graham. 2015. Margination regimes and drainage transition in confined multicomponent suspensions. *Phys. Rev. Lett.* 114:188101.

37. Kumar, A., and M. D. Graham. 2012. Margination and segregation in confined flows of blood and other multicomponent suspensions. *Soft Matter.* 8:10536–10548.

38. Fitzgibbon, S., A. P. Spann, …, E. S. G. Shaqfeh. 2015. In vitro measurement of particle margination in the microchannel flow: effect of varying hematocrit. *Biophys. J.* 108:2601–2608.

39. Tan, J., A. Thomas, and Y. Liu. 2011. Influence of red blood cells on nanoparticle targeted delivery in microcirculation. *Soft Matter.* 8:1934–1946.

40. Barbee, J. H., and G. R. Cokelet. 1971. The Fahraeus effect. *Microvasc. Res.* 3:6–16.

41. Brizel, D. M., B. Klitzman, …, M. W. Dewhirst. 1993. A comparison of tumor and normal tissue microvascular hematocrits and red cell fluxes in a rat window chamber model. *Int. J. Radiat. Oncol. Biol. Phys.* 25:269–276.

42. Amin, T. M., and J. A. Sirs. 1985. The blood rheology of man and various animal species. *Q. J. Exp. Physiol.* 70:37–49.

43. MacEwan, S. R., D. J. Callahan, and A. Chilkoti. 2010. Stimulus-responsive macromolecules and nanoparticles for cancer drug delivery. *Nanomedicine (Lond.).* 5:793–806.

44. Kubota, K., J. Tamura, …, I. Nishio. 1996. The behaviour of red cells in narrow tubes in vitro as a model of the microcirculation. *Br. J. Haematol.* 94:266–272.

45. Cai, B., J. Fan, …, B. M. Fu. 2012. Adhesion of malignant mammary tumor cells MDA-MB-231 to microvessel wall increases microvascular permeability via degradation of endothelial surface glycocalyx. *J. Appl. Physiol.* 113:1141–1153.

46. Pries, A. R., T. W. Secomb, and P. Gaehtgens. 1995. Structure and hemodynamics of microvascular networks: heterogeneity and correlations. *Am. J. Physiol.* 269:H1713–H1722.

47. Klug, P. P., L. S. Lessin, and P. Radice. 1974. Rheological aspects of sickle cell disease. *Arch. Intern. Med.* 133:577–590.

48. Son, Y. 2007. Determination of shear viscosity and shear rate from pressure drop and flow rate relationship in a rectangular channel. *Polymer (Guildf.).* 48:632–637.

49. Reasor, D. A., Jr., M. Mehrabadi, …, C. K. Aidun. 2013. Determination of critical parameters in platelet margination. *Ann. Biomed. Eng.* 41:238–249.

50. Einstein, A. 1905. Über die von der molekularkinetischen Theorie der Wärme geforderte Bewegung von in ruhenden Flüssigkeiten suspendierten Teilchen. *Ann. Phys.* 322:549–560.

51. Ahmad, T., and I. Hassan. 2010. Experimental analysis of microchannel entrance length characteristics using microparticle image velocimetry. *J. Fluids Eng.* 132:041102.

52. Katanov, D., G. Gompper, and D. A. Fedosov. 2015. Microvascular blood flow resistance: role of red blood cell migration and dispersion. *Microvasc. Res.* 99:57–66.

53. Kumar, A., and M. D. Graham. 2012. Mechanism of margination in confined flows of blood and other multicomponent suspensions. *Phys. Rev. Lett.* 109:108102.

54. Sutherland, W. 1905. LXXV. A dynamical theory of diffusion for non-electrolytes and the molecular mass of albumin. *Phil. Mag.* 9:781–785.

55. Lopez, M., and M. D. Graham. 2007. Shear-induced diffusion in dilute suspensions of spherical or nonspherical particles: effects of irreversibility and symmetry breaking. *Phys. Fluids.* 19:073602.

56. Zhao, H., E. S. G. Shaqfeh, and V. Narsimhan. 2012. Shear-induced particle migration and margination in a cellular suspension. *Phys. Fluids.* 24:011902.

57. Hashizume, H., P. Baluk, …, D. M. McDonald. 2000. Openings between defective endothelial cells explain tumor vessel leakiness. *Am. J. Pathol.* 156:1363–1380.

58. Wiedeman, M. P. 1963. Dimensions of blood vessels from distributing artery to collecting vein. *Circ. Res.* 12:375–378.